Canadian Journal of Physics

FERMILAB-PUB-24-0306-LBNF

OPEN ACCESS | Review

Neutrino oscillations

Deborah A. Harris[a,b], **Nikolina Ilic**[c,d], **and Akira Konaka**[e]

[a]Department of Physics and Astronomy, York University, Toronto, ON, Canada; [b]Fermi National Accelerator Laboratory, Batavia, IL, USA; [c]Department of Physics, University of Toronto, Toronto, ON, Canada; [d]Institute of Particle Physics, Victoria, BC, Canada; [e]TRIUMF, Vancouver, BC, Canada

Corresponding author: **Deborah A. Harris** (email: deborahh@yorku.ca)

Abstract

Neutrino oscillation measurements provide an important window on what lies beyond the Standard Model of particle physics. These measurements may unlock the mechanism by which the universe came to become matter-dominated, and may offer hints of another mechanism to generate particles with mass. Measurements of oscillations from muon neutrinos to electron neutrinos (and their antineutrino counterpart) as a function of time provide critical inputs to understanding both mechanisms. These are challenging measurements and a variety of techniques and strategies are required to get the complete picture. This article describes the current status of our understanding of neutrino masses and how neutrinos oscillate between one flavour and another as they propagate through space and time, and what remains to be understood. Taking the next steps in this field requires a variety of approaches and a better understanding of how neutrinos interact with nuclei. This article describes two of those next steps, highlighting where Canadian groups are active, and concludes with a discussion of the broad range of additional physics that becomes accessible by having two very different large sensitive neutrino detectors making these measurements.

Key words: neutrino, neutrino detectors, neutrino interactions, neutrino oscillations, CP violation

1. Introduction

Neutrinos are neutral subatomic particles that interact only through weak interactions, and are therefore insensitive to either the electromagnetic or the strong force. The weak interaction distinguishes neutrino flavours, or weak eigenstates ν_e, ν_μ, ν_τ through their couplings to charged leptons: electrons, muons, and taus. While neutrinos travel through space, however, they travel as mass eigenstates, unimaginatively called ν_1, ν_2, and ν_3. These two sets of eigenstates, ν_e, ν_μ, and ν_τ and ν_1, ν_2, and ν_3 can be related through a mixing matrix, which is expected to be unitary.

In the case of quarks, the fact that the weak eigenstates and the mass eigenstates are different is naturally understood because the Higgs mechanism, which produces quark masses, is different from the weak interaction. This allows, for example, kaons, which contain second-generation strange quarks, to decay into pions with first-generation quarks. Because quarks have significant and significantly different masses they become their mass eigenstates immediately.

On the other hand, the very light neutrino masses allow neutrinos to travel as a coherent sum of three mass eigenstates. Since the time evolution of the quantum phase of particles is proportional to the energy of the particle, the phases for different mass eigenstates evolve differently, which creates a combination of flavour eigenstates that not only change but oscillate as a function of time. This phenomenon is called neutrino oscillations.

The probability for neutrinos to oscillate is governed by the masses of the neutrinos, m_1, m_2, m_3, and the mixing between the weak and mass eigenstates, which is described by the Pontecorvo–Maki–Nakagawa–Sakata matrix. Because the mixing matrix must be unitary, it can be parametrized by three mixing angles, θ_{12}, θ_{23}, and θ_{13}, and one complex phase denoted δ. Since the δ is replaced by $-\delta$ for antiparticles, the phase introduces a particle–antiparticle asymmetry in neutrino oscillation; in other words charge–parity (CP) vio-

lation. One common parameterization of this matrix is given below:

$$\begin{pmatrix} \nu_e \\ \nu_\mu \\ \nu_\tau \end{pmatrix} = \begin{pmatrix} U_{e1} & U_{e2} & U_{e3} \\ U_{\mu 1} & U_{\mu 2} & U_{\mu 3} \\ U_{\tau 1} & U_{\tau 2} & U_{\tau 3} \end{pmatrix} \begin{pmatrix} \nu_1 \\ \nu_2 \\ \nu_3 \end{pmatrix} = \begin{pmatrix} 1 & 0 & 0 \\ 0 & \cos\theta_{23} & \sin\theta_{23} \\ 0 & -\sin\theta_{23} & \cos\theta_{23} \end{pmatrix} \times \begin{pmatrix} \cos\theta_{13} & 0 & \sin\theta_{13}e^{-i\delta} \\ 0 & 1 & 0 \\ -\sin\theta_{13}e^{i\delta} & 0 & \cos\theta_{13} \end{pmatrix} \times \begin{pmatrix} \cos\theta_{12} & \sin\theta_{12} & 0 \\ -\sin\theta_{12} & \cos\theta_{12} & 0 \\ 0 & 0 & 1 \end{pmatrix} \begin{pmatrix} \nu_1 \\ \nu_2 \\ \nu_3 \end{pmatrix} \quad (1)$$

When a ν_μ travels as a superposition of mass eigenstates, m_1, m_2, and m_3 with their nearly identical energies of E_1, E_2, and E_3, its survival probability as a function of distance L can be described using a similar formalism as in a double-slit interference pattern with light. Given the mass differences that have been measured, the ν_μ survival probability at relatively short distances is to first order a function of the larger mass splitting, which is the difference between m_2^2 and m_3^2 (or Δm_{32}^2). This means that it is also mostly a function of one of the mixing angles in the PMNS matrix, θ_{23}(see ref. [1]), for example:

$$P\left(\nu_\mu \to \nu_\mu\right) \simeq 1 - \sin^2 2\theta_{23} \sin^2 \frac{1.27\Delta m_{32}^2\,(\mathrm{eV}^2)\,L\,(\mathrm{km})}{E_\nu\,(\mathrm{GeV})} \quad (2)$$

This was the muon neutrino disappearance that was discovered in atmospheric neutrinos by the Super-Kamiokande (SuperK) detector, which saw that muon neutrinos that traveled through the earth to the detector were not as likely to survive relative to the muon neutrinos that were produced directly above the detector [2]. This result demonstrated that at least one of the neutrinos must have a mass, and that the weak and mass eigenstates must be different from one another. The Sudbury Neutrino Observatory (SNO) experiment, by studying solar neutrinos, was able to see ν_e from the sun changing to other flavours by measuring separately the total neutrino and the electron neutrino flux [3]. These two measurements implied that there must be at least two nonzero neutrino masses, and at least two nonzero mixing angles. The fact that these two mixing angles are already much larger than those in the CKM matrix describing quarks is a hint that the source of mixing in the lepton sector may be independent of the source of mixing in the quark sector. Between the time of these first discoveries and now, there have been successively more precise measurements of the mixing angles, both with naturally occurring neutrinos, and with neutrinos from reactors [4–6] and accelerators [7, 8].

However, in order to see whether there is CP violation, it is not sufficient to measure survival probabilities, experiments must measure neutrinos changing from one flavour to another. This is because of CPT invariance, since that implies that the probability of $\nu_x \to \nu_x$ must equal the probability of $\bar{\nu}_x \to \bar{\nu}_x$. Accelerators can produce neutrino beams that are over 95% pure ν_μ or $\bar{\nu}_\mu$, with little contamination from other flavours. Therefore, a measurement of $\nu_\mu \to \nu_e$ can be made, and then compared with a similar measurement of $\bar{\nu}_\mu \to \bar{\nu}_e$ to search for CP violation.

When neutrino beams are sent through the earth, however, there is an interaction with the electrons in the earth that changes the propagation from that of pure mass eigenstates. This is because electron neutrinos and antineutrinos can scatter off the electrons in the earth through a charged current (CC) interaction, while the muon and tau neutrinos cannot [9]. In the analogy of a double slit experiment, the earth electrons act as a flavour slit, which modifies the neutrino oscillation phase. This effect, called a "matter effect", grows with the distance that the neutrinos have traveled. This means that even if there were no CP-violating phase in the mixing matrix, there would still be a difference between neutrino and antineutrino oscillation probabilities $P(\nu_\mu \to \nu_e)$ and $P\left(\bar{\nu}_\mu \to \nu_e\right)$, because the electrons in the earth are particles and not antiparticles.

Given the mixing matrix described above and matter effects, the equation that describes electron neutrino appearance in a muon neutrino beam as a function of the distance traveled (L) has several terms, which at some distances may have similar sizes, and is given in the equation below [1]:

$$\begin{aligned} P_{\nu_\mu \to \nu_e(\bar{\nu}_\mu \to \bar{\nu}_e)} \simeq\ & 4\sin^2\theta_{13}\sin^2\theta_{23}\frac{\sin^2\Delta\,(1 \mp A)}{(1 \mp A)^2} \\ & + \alpha^2 \sin^2 2\theta_{12}\cos^2\theta_{23}\frac{\sin^2 A\Delta}{A^2} \\ & + 8\alpha J_{\mathrm{CP}}^{\max}\cos\left(\Delta \pm \delta\right)\frac{\sin\Delta A}{A}\frac{\sin\Delta\,(1 \mp A)}{1 \mp A} \end{aligned} \quad (3)$$

Here, $\alpha = \frac{\Delta m_{21}^2}{\Delta m_{31}^2} \simeq 0.03$, $\Delta = \frac{\Delta m_{31}^2 L}{4E_\nu}$, and $A = \frac{2E_\nu V}{\Delta m_{31}^2} \sim 0.1E_\nu\,(\mathrm{GeV})$ where V is the effective matter potential in the earth crust, and $J_{\mathrm{CP}}^{\max} = \cos\theta_{12}\sin\theta_{12}\cos\theta_{23}\sin\theta_{23}\cos\theta_{13}\sin\theta_{13}$ is the maximum value of Jarlskog CP invariant [10]. The δ_{CP} and A change sign to $-\delta_{\mathrm{CP}}$ and $-A$ for the antineutrino case as shown in the formula. Using the known mixing angle values, the leading θ_{13} term, the first term of the first line in eq. (2) becomes 0.044 at the oscillation maximum of $\Delta = \pi/2$. This significant θ_{13} mixing angle between first and third generation was a

surprise when T2K found evidence in 2011 [11] and Daya Bay discovered it in 2012 [12]. The Jarlskog invariant, J_{CP}^{max}~0.033 is large compared to quark case thanks to the significant size of the mixing angles, $\theta_{12} \sim 33^\circ$, $\theta_{23} \sim 45^\circ$, and $\theta_{13} \sim 8.5^\circ$. For the maximum CP violation case of $\delta = \pi/2$, the CP-violating term is as large as 0.0124, which is 28% of the leading θ_{13} term for $\nu_\mu \rightarrow \nu_e$ appearance, opening a possibility of studying CP violation in neutrino oscillations. The matter effect (A term) creates additional neutrino–antineutrino asymmetry of ~10% for $E_\nu = 0.6$GeV and $L = 300$ km (HyperK oscillation maximum) and ~50% for $E_\nu = 2.6$GeV and $L = 1300$ km (Deep Underground Neutrino Experiment (DUNE) oscillation maximum). These two baselines correspond to the two different experimental approaches described below.

For distances of 300 km, this matter asymmetry is expected to be smaller than the largest possible CP-violating difference and have less impact on the CP violation measurement. On the other hand, for a distance of 1300 km, the matter effect is expected to be larger than the largest possible CP-violating difference. The benefit of measuring this effect is that while the size of the neutrino–antineutrino difference is already known from the density of electrons in the earth and the Fermi coupling constant, whether the difference is positive or negative depends on whether m_3 is greater than or less than m_2 and m_1 (normal or inverted ordering, respectively). Most models for neutrino mass predict a "normal" hierarchy or ordering, since that would mean that there is one heavy mass eigenstate and two light ones, similar to the charged fermion mass spectra. However, if neutrino masses are in an "inverted" ordering, then this would increase the neutrinoless double beta decay rate that would be expected.

There are two different strategies for pursuing this physics, both of which which are currently underway in Canada: one strategy is to maximize statistics at the oscillation maximum, and the other is to maximize the event rate over a broad energy spectrum to measure the oscillation probability as a function of neutrino energy. These two strategies imply drastically different choices of beam energies and detector technologies, as we will describe in the remainder of this article. The Hyper-Kamiokande (HyperK) experiment, hosted in Japan, is an upgrade to the currently operating Tokai-to-Kamiokande (T2K) experiment, and both have a narrow energy beam peaked at 600 MeV and a baseline of 295 km, while DUNE, hosted in the United States, will use a broad energy range of neutrino energies (1–5 GeV) at a baseline of 1300 km.

Figure 1 illustrates the comparable sizes of different oscillation components by showing the breakdown of the $\nu_\mu \rightarrow \nu_e$ oscillation probability as a function of neutrino energy at 295 km: the CP-conserving and CP-violating contributions in eq. (2) for $\delta_{CP} = \pi/2$ are shown separately. The CP violation contribution at the peak oscillation energy may be as large as 28% thanks to the large mixing angles, θ_{13}, θ_{12}, and θ_{23} as shown in eq. (2). By comparing $\nu_\mu \rightarrow \nu_e$ and $\bar{\nu}_\mu \rightarrow \bar{\nu}_e$, which corresponds to the two $\pm$ sign options in eq. (2), long baseline oscillation experiments can measure the neutrino mass ordering and are uniquely sensitive to the CP-violating phase δ.

Fig. 1. Top: $\nu_\mu \rightarrow \nu_e$ oscillation probability as a function of neutrino energy for neutrinos that have traveled 295 km, broken into the first (leading) term in eq. (2), the size of the matter effects, and the CP-conserving (CPC) and CP-violating (CPV) components present in the last two terms in eq. (2). Middle: Neutrino flux at different off-axis directions. Bottom: Neutrino cross section divided by energy as a function of neutrino energy for the charged current quasielastic (CCQE) process, charged and neutral current single pion production (CC1π and NC1π) [13].

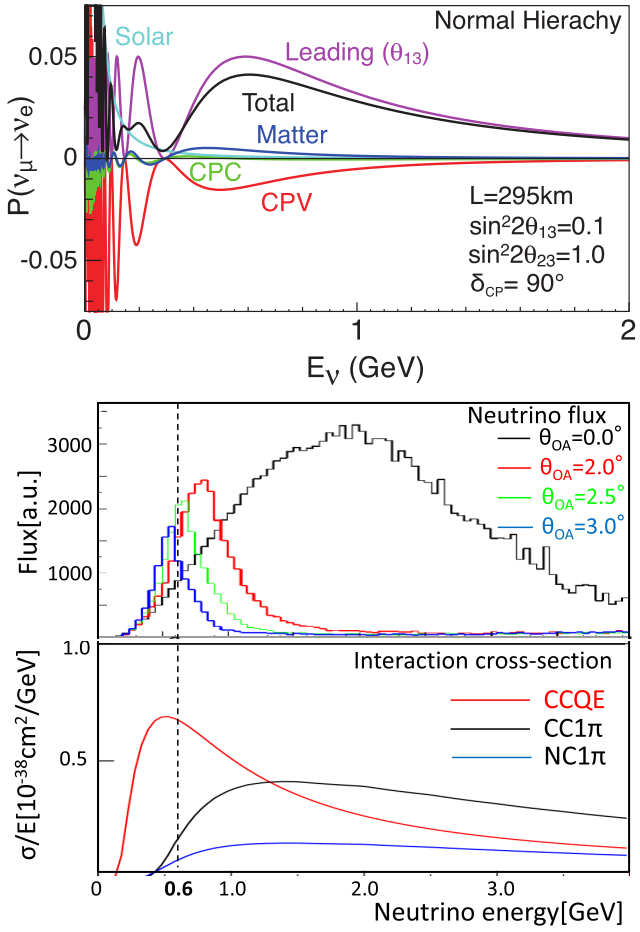

2. Long baseline neutrino oscillation method

Long baseline neutrino oscillation measurements are performed by producing a well-understood neutrino beam that is detected hundreds of kilometers away from where the neutrinos are produced. The detector must measure both the flavour and energy of the neutrinos in the beam in order to extract the oscillation probabilities. Because the event rates as a function of the neutrino flux, cross section, and detector acceptance are difficult to predict absolutely, the event rates at the far detector are compared to those at a detector located close to the neutrino production point, before oscillations have occurred. In this section, the ingredients needed for the oscillation measurement are described: neutrino beams, neutrino detectors, and a few recent neutrino

interaction cross section measurements, with a focus on where Canadian groups are participating.

2.1. Production of neutrino beams

Neutrino beams are produced when a high-energy proton beam hits a target to produce pions, which are then focused using toroidal field magnets ("horns") [14] and sent to a decay region where they decay primarily to muons and muon neutrinos or muon antineutrinos depending on the charge of pion that is focused. The toroidal field makes a point-to-parallel focus for positively charged particles and defocuses for negatively charged particles and vice versa depending on the polarity of the current the horns. By focusing positive or negative pions, a primarily neutrino or antineutrino beam is produced. Multiple horn magnets are used to focus a wider range of pion momenta, similar to using multiple lenses on cameras to achieve an achromatic focus.

The neutrino beam intensity is the highest in the direction that the horns focus the pions to travel. In this case, the neutrino energy will be about 40% of the parent pion energy and have a wide energy distribution (referred to as a wide-band beam). DUNE will take advantage of this to maximize the total neutrino event rate. When the detector is placed slightly away from the beamline axis, the two body decay kinematics of pions results in a quasimonochromatic beam (off-axis beam) [15]. Higher momentum pions produce higher energy neutrinos, whereas the Lorentz boost suppresses higher energy neutrinos from being produced at a larger angle. This off-axis technique can be used to enhance the neutrino flux at the oscillation maximum and suppress backgrounds from higher energy neutrinos as shown in Fig. 1 (right). For T2K and HyperK, the direction of the proton beam and the toroidal horn magnets axis are intentionally displaced by an off-axis angle of 2.5 degrees from the neutrino detector direction.

This suppression is important for the kinematic neutrino energy reconstruction, as will be discussed later. The off-axis beam configuration also makes the neutrino beam flux less sensitive to the parent pion momentum, which reduces the a priori neutrino flux uncertainties. Figure 2 shows the DUNE (top) and T2K and HK fluxes (bottom), along with the ν_e appearance probability from the leading term and CP-violating term for distances of both 1300 km (top) and 295 km (bottom), for both the "normal" and "inverted" mass ordering.

2.2. Neutrino detectors

Neutrino interactions on nuclei can produce charged particles, in particular charged leptons associated with the neutrinos through charged current (CC) interactions. For example, muon neutrinos produce μ^-, whereas electron neutrinos produce e^-. For neutrino energies at about 1 GeV, most interactions are quasielastic; namely a neutrino converts to a negatively charged lepton, and neutron converts to a proton. For antineutrino interactions, a positively charged lepton is produced, but in this case, an initial state proton is converted to a neutron. Different detector technologies are sensitive to different final state particles, but in either case the key to

Fig. 2. Neutrino fluxes for the Deep Underground Neutrino Experiment (DUNE) (top) and HyperK (bottom) oscillation experiments, along with the electron neutrino appearance probability as a function of neutrino energy for that baseline. "NO" and "IO" refer to the normal and inverted mass ordering, and three different values of the CP-violating phase δ are shown. Images courtesy C. Wret, using 2022 world average oscillation parameters from NuFit 5.2 [16] with the program in ref. [17], updated from ref. [18].

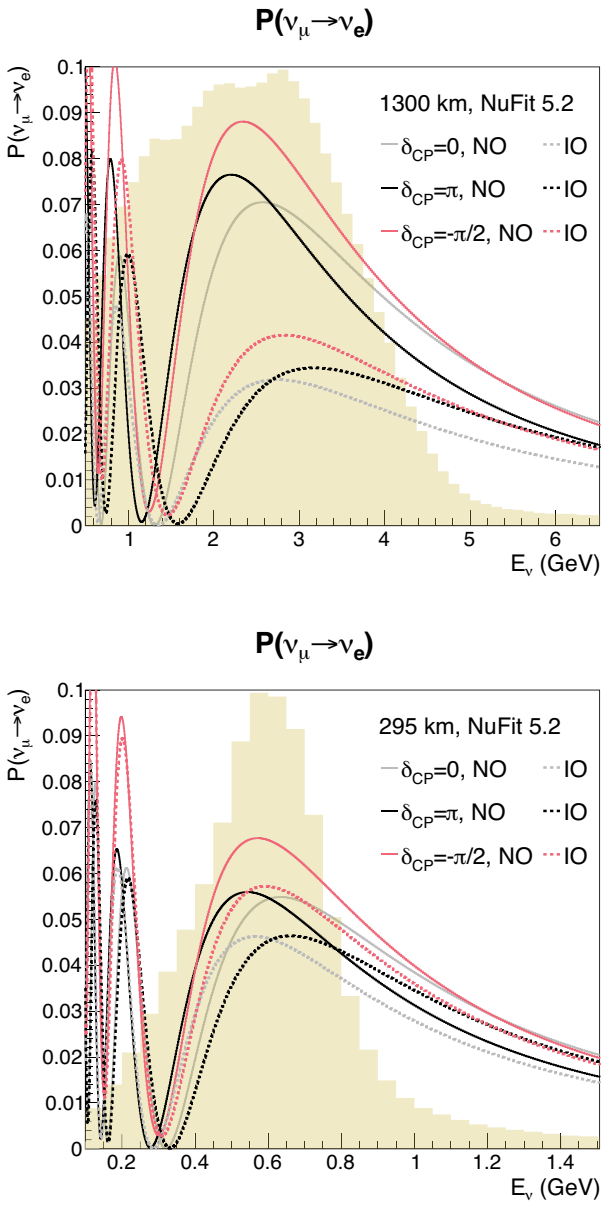

measuring oscillations is getting the incoming flavour and estimating the energy of the neutrino.

As the neutrino energy increases, the energy that can be transferred to the nucleus increases, and therefore, the number of final state particles increases from just one lepton and one nucleon to several final state hadrons. The choice of detector technology is informed by the neutrino en-

ergy the experiment wishes to measure, as described in this section.

2.2.1. Water Cerenkov detector

When a charged particle travels in water at a speed faster than the speed of light in the water, which is $1/n = 1/1.33$ of the speed of light in vacuum, Cherenkov light is emitted at a specific angle, creating a ring of light at the wall of a detector. This Cherenkov ring carries the information about the direction, energy, and identity of the charged particle. The ring shape becomes fuzzy for electrons and γs due to the development of the electromagnetic shower in the water, and can be separated from rings from muons, which have sharp edges (as shown in Fig. 3). Pions and protons above the Cherenkov threshold (for which $v > c/n$) go through hadronic scatterings in the water, making a multi-ring signature. These ring patterns are used for particle identification. Figure 3 shows simulated events in the SuperK detector for an electron and a muon neutrino CC interaction.

Large Water Cerenkov detectors have a history of discoveries. The original Kamiokande detector, constructed to search for proton decays predicted by the Grand Unification model, saw deficits in both the solar and atmospheric neutrino event rates [19, 20], which led to the discovery of the atmospheric and solar neutrino oscillations by SuperK [2] and the SNO [3]. Kamiokande (along with IMB) also discovered supernova neutrinos from the Large Magellanic Cloud SN1987A [21, 22], confirming that the neutrino wind drives the supernova explosion.

Because of the relatively high momentum thresholds for seeing hadrons (137 MeV/c for pions and 1300 MeV/c for protons), the Water Cerenkov technology is not a good calorimeter for hadrons. However, the neutrino energy can be approximated by measuring the charged lepton momentum vector with respect to the known incoming neutrino direction and assuming two body charged current quasielastic (CCQE) kinematics, $\nu_\mu n \rightarrow \mu^- p$. This approach is effective in the sub-GeV neutrino energy where CCQE cross-section dominates as shown in Fig. 1 (right). Because the target neutrons are bound inside the oxygen nucleus, the reconstructed energy is subject to additional smearing beyond that due to detector resolution, as described in ref. [23].

2.2.2. Liquid argon time projection chamber

The liquid argon Time Projection Chamber technology works by generating a large electric field in a volume of liquid argon, and then instrumenting that volume by placing either wires or pixels on the surface that can receive a signal when the ionized electrons drift to the wires or pixels. These active elements can be located meters away from where the neutrino interacted. The arrival time of the drifting electrons is related to the distance the charged particle was from the readout planes. Figure 3 shows an event display from MicroBooNE [24], which took data in a wide band 1 GeV beam at Fermilab. In this way, one can instrument a kton-scale detector with mm-scale granularity with a manageable number of readout channels. The argon must be pure so that the ionized electrons are not absorbed, for example, by oxygen or other impurities. Charged particles that pass through the argon will also produce scintillation light, which is also collected on the edges of the active volume of argon [25].

The liquid argon TPC technology was pioneered by ICARUS [26] at CNGS and employed at Fermilab by MicroBooNE [24] to study neutrinos from a few dozen GeV to a few hundred MeV in energy respectively, and is being further developed by the Short Baseline Neutrino Detector collabora-

Fig. 3. Top and middle: two data event displays from the Super-Kamiokande detector from neutrinos that originated in the T2K neutrino beamline. The bright green circles represent PMT hits from Cherenkov light that arrives within 16 ns after correction for travel distance from the event vertex. The size of the circle represents the number of photoelectrons. The pink diamond is directed from the event vertex along the T2K beam direction. The upper figure is a single-ring muon event with muon momentum 640 MeV/c; the middle figure is a single-ring electron event with electron momentum 630 MeV/c. Images courtesy of the Super-K and T2K collaborations. Bottom: a data event display from the MicroBooNE liquid argon detector from an electron neutrino that originated in the NuMI beamline. The measured electron energy is 2.07 GeV and the total measured visible energy is 2.50 GeV. Image courtesy of the MicroBooNE collaboration.

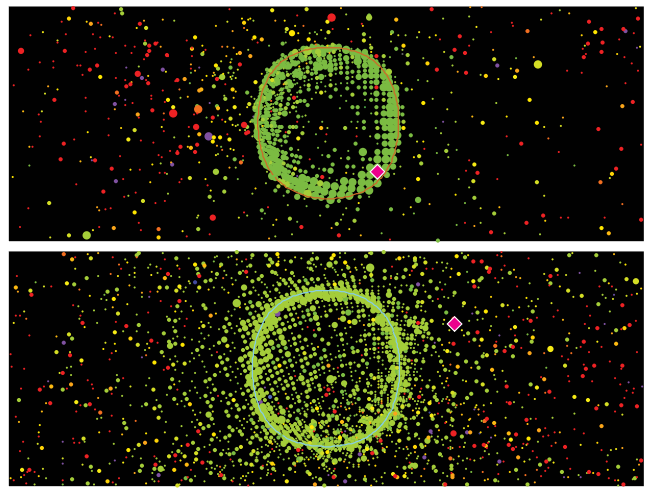

tion at Fermilab [27]. This technology has much lower thresholds for particle detection than the Water Cerenkov technology, and there is significantly more information about each neutrino interaction. The higher energy neutrinos at DUNE will produce many more final state particles than the lower energy neutrinos at HyperK, so the ability to see these final state particles is crucial to infer neutrino energies. Based on these considerations and the success of ICARUS, LAr TPC technology has been chosen for the DUNE experiment [28]. The community's expertise in using this detector technology is rapidly expanding given the test beam programs at CERN [25] and Fermilab [29], and MicroBooNE, and the field is starting to see the role that machine learning can play in analyzing these detailed images of neutrino interactions [30, 31].

2.3. Neutrino interactions

For accelerator-based neutrinos, the incoming neutrino direction is known given the location of the neutrino interaction point in the detector and the average pion decay location in the beamline. The only way an experiment can estimate the neutrino energy is through the final state particles produced in the interaction. Since the neutrino oscillation probability is a function of the neutrino energy, energy reconstruction is essential in neutrino oscillation measurements. There are two common approaches to neutrino energy reconstruction: kinematic reconstruction where only the final state lepton momentum and angle with respect to the neutrino beam is measured and a two-body reaction is assumed (for example, $\nu_\mu n \rightarrow \mu^- p$), and calorimetric reconstruction, where leptonic and hadronic energy deposits in the final state are summed. In both cases assumptions must be made.

For kinematic reconstruction, the assumptions are the interaction process, the binding energy of the nucleons, and the initial state nucleon momentum. In calorimetric reconstruction, the most important assumptions concern the energy that is lost to particles that do not leave their kinetic (or total) energies in the detector, which must be estimated. Kinematic reconstruction is appropriate for sub-GeV neutrinos where the CCQE reaction dominates the event rate, so measurement of final state hadrons is not required. This reconstruction has an associated uncertainty due to nuclear effects, which modify the initial nucleon momenta and their binding energies, and provide processes that involve initial state correlated nucleons in the nucleus rather than just a single nucleon. The calorimetric method works at higher energy where the CCQE reaction is not the dominant interaction (see Fig. 1). The challenge is to estimate the energy carried by final state neutrons, particularly in the case of antineutrino interactions where the recoil particles typically include neutrons. Both for kinematic and calorimetric approaches, the neutrino interaction cross section model uncertainty has a significant impact.

Preparing for the next generation of experiments means not only figuring out how to scale up current detector technologies, but also means making better measurements of neutrino interactions to improve the models that the next generation of experiments use. The MINERvA experiment, which ran at Fermilab between 2009 and 2019, was designed

Fig. 4. Form factor measured using antineutrino scattering off free protons, shown as a ratio to the dipole form factor, taken from ref. [38].

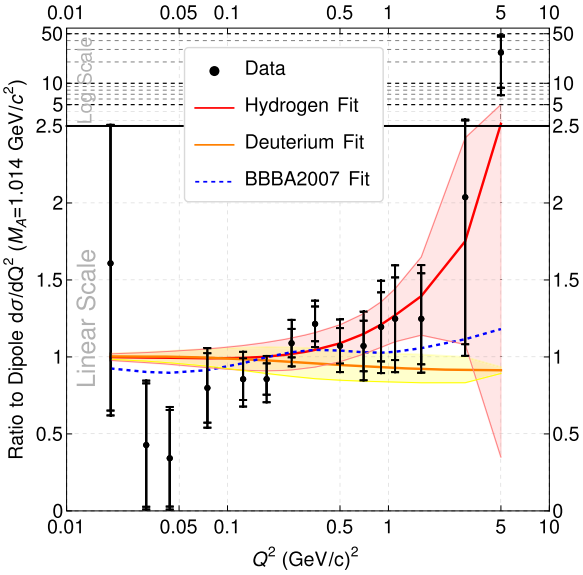

to measure a variety of neturino interaction channels on a broad range of target nuclei. Canadian efforts started on this experiment in 2019 and have resulted in several recent publications that have direct applications for neutrino oscillation experiments. Two of those measurements are described in this section, but a longer list of recent publications with Canadian participation can be found in refs. [32–37].

A measurement of antineutrino quasielastic scattering on hydrogen was performed by scattering off plastic scintillator that is largely CH, and then subtracting off the background of scattering from Carbon [38]. The background was constrained by MINERvA's own data, by taking advantage of the same nuclear effects that modify the reconstructed neutrino energy for Water Cerenkov detectors. The events on hydrogen can be used to measure the form factor of the free nucleon, which governs the cross section prediction. In current models of quasielastic interactions, the form factor as a function of momentum transfer squared (Q^2) was assumed to be a dipole form, which is simply the Fourier transform of a uniform charge distribution. However, recent analyses have shown that this assumption underestimates the uncertainty at high Q^2 [39]. This improved measurement of the nucleon form factor, shown in Fig. 4, is more in agreement with lattice QCD predictions, and provides a substantial improvement over the previous low statistics measurements using deuterium.

The way that the neutrino energy is reconstructed is different between Water Cerenkov detectors and the active calorimetric detectors, as described above. One way to test models that is of direct relevance to oscillation experiments is to compare the kinematic to calorimetric reconstruction for the same events in both data and models. Since the lepton energy reconstruction is the same, the clearest difference will be in the extra energy that is added to the lepton energy to estimate the neutrino energy.

Fig. 5. Measured cross section as a function of the calorimetric extra energy (sum of proton kinetic energy, or ΣT_p), compared with predictions shown for different quasielastic-like interactions where there are no pions in the final state, for different bins of extra energy evaluated using muon kinematics (using a quasielastic hypothesis, or $q_0^{(QE)}$), taken from ref. [40].

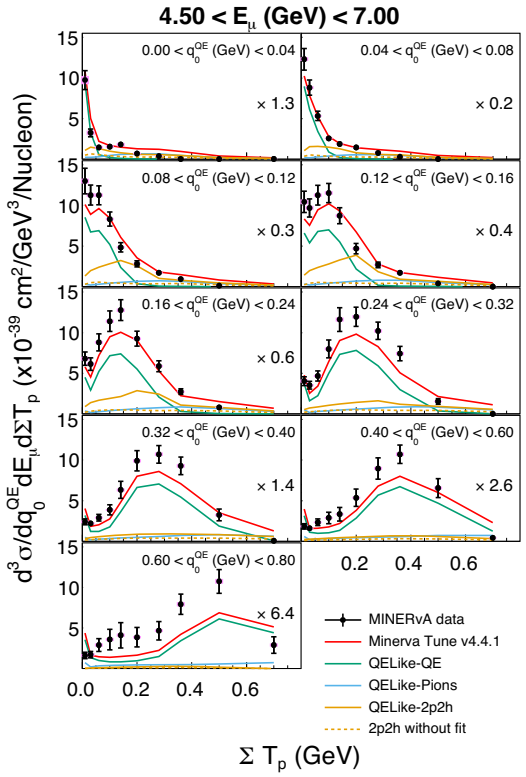

For Cherenkov-based detectors, this extra energy, $q_0^{(QE)}$, is given by the following formula:

$$q_0^{(QE)} \equiv \frac{m_p^2 - (m_n - E_b)^2 - m_\mu^2 + 2\left(E_\mu - p_\mu \cos\theta_\mu\right) E_\mu}{2\left(m_n - E_b\right) - E_\mu + p_\mu \cos\theta_\mu} \tag{4}$$

For calorimetric reconstruction of quasielastic events, the extra energy is dominated by the total kinetic energy of the final state protons, although there may still be missed energy from neutrons or photons that escape the detector without interacting. The MINERvA experiment can measure both the total proton kinetic energy and $q_0^{(QE)}$ simultaneously, as described in ref. [40]. Figure 5 shows the cross section for the kinematic extra energy reconstruction as a function of the calorimetric extra energy. The fact that the model does not reproduce the data means that a larger uncertainty on that model should be included, otherwise using this model may result in two different sets of oscillation parameters for the same data set but with different energy reconstruction techniques.

The T2K collaboration has also recently produced a number of neutrino cross section measurements, again with significant Canadian leadership, and are provided in refs. [41–44]

Fig. 6. Muon neutrino (top) and antineutrino (bottom) events (measured and predicted by the best three-generation oscillation fit results) as a function of the reconstructed neutrino energy.

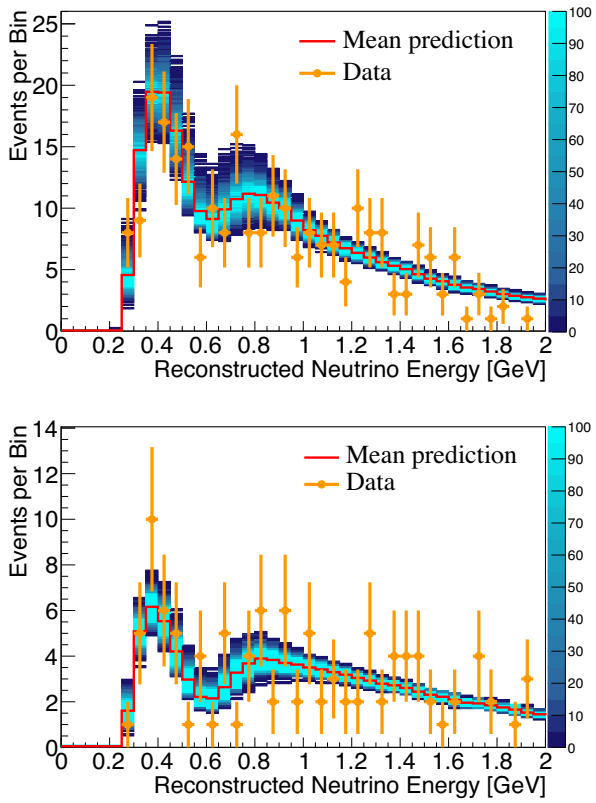

3. Current neutrino oscillation measurements

The T2K long baseline neutrino experiment is currently operating and has had significant Canadian involvement since its inception [45], with a focus on the design and construction of the neutrino beam facility and the near detector complex (ND280) [46]. T2K's neutrino beam is produced on the east coast of Japan, monitored by a near detector complex and then goes through the earth 295 km to the SuperK detector near the west coast of Japan. Figure 6 shows the muon neutrino disappearance signature observed by the T2K experiment [8, 47]. A clear oscillation pattern is observed. The dip position at 0.6 GeV in the reconstructed neutrino energy is a function of Δm^2_{32} and the depth of the dip is a function of the mixing angle $\sin^2\theta_{23}$.

The observed mixing angle θ_{23} is consistent with the maximal mixing $\sin^2 2\theta_{23} = 1$. The large θ_{23} value, when first seen in atmospheric neutrino mixing was surprising since it was so different from the small quark mixing angles. If the signature for maximal mixing persists, this may indicate an underlying symmetry between the muon and tau neutrinos. The measurement of θ_{23} is ultimately limited by the systematic uncertainty in neutrino interactions, which cause higher energy neutrino events to be reconstructed with lower neutrino energy and fill in the dip in the event spectra. In HyperK and

Fig. 7. Examples of electron neutrino (top) and antineutrino (bottom) appearance signatures measured by the Tokai-to-Kamiokande (T2K) experiment.

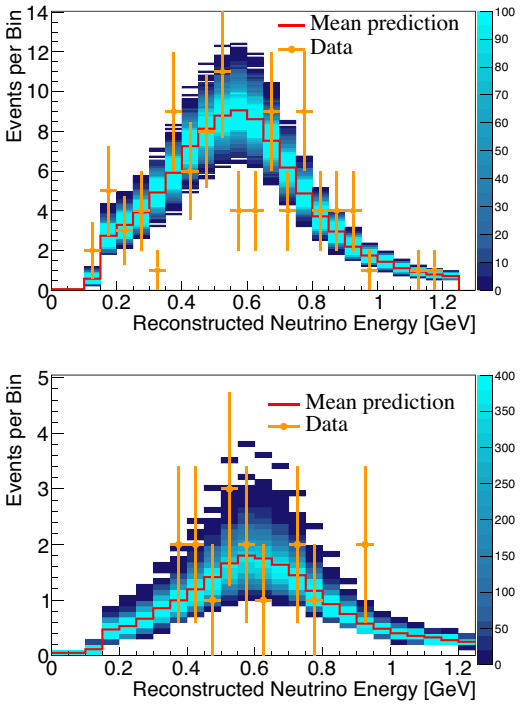

DUNE, this uncertainty will be reduced by taking near detector measurements at several angles, which result in several different energy spectra, as will be discussed in Section 5.

The measurement of the sign of $\Delta m^2_{32} \equiv m^2_3 - m^2_2$ is sensitive to the neutrino mass ordering of ν_3 and $\nu_{1,2}$ [48, 49]. The ν_2 mass is larger than ν_1 as measured in the solar neutrino oscillations, but whether the ν_3 mass is larger (normal ordering) or smaller than $\nu_{1,2}$ (inverted ordering) is not known yet. $|\Delta m^2_{32}|$ is less than $|\Delta m^2_{31}|$ for the normal ordering, whereas $|\Delta m^2_{32}|$ is greater than $|\Delta m^2_{31}|$ for inverted ordering. The difference is $\left(\Delta m^2_{31} - \Delta m^2_{32}\right)/\Delta m^2_{32} = \Delta m^2_{21}/\Delta m^2_{32} = 7.5 \times 10^{-5} eV^2/2.5 \times 10^{-3} eV^2 \sim 3\%$. The reactor neutrino $\bar{\nu}_e$ disappearance measures $|\Delta m^2_{31}|$ and the current Daya Bay uncertainty is 2.4% for the normal mass ordering [4]. The JUNO experiment plans to measure $|\Delta m^2_{31}|$ with 0.8% precision in the first 100 days of operation and projects to reach 0.2% after 6 years [50]. Both the T2K and NOvA ν_μ disappearance measure $|\Delta m^2_{32}|$ with an uncertainty of about 2% [7, 8]. Both DUNE and HyperK aim to measure $|\Delta m^2_{32}|$ to 0.4% and 0.6%, respectively, through better statistics and the improved near detector strategy, as will be described later [13, 51].

T2K has observed the neutrino flavour transitions from ν_μ to ν_e and $\bar{\nu}_\mu \to \bar{\nu}_e$. Figure 7 shows the reconstructed ν_e and $\bar{\nu}_e$ energy spectra observed in T2K. The peak positions is again a function of $|\Delta m^2_{31}|$, and the size of the peak is primarily a function of $\sin^2 2\theta_{13}$, the leading term in eq. (2). To see whether there is sensitivity to a CP-violating phase, an average value of θ_{13} from reactors is used. Given that constraint, the CP-conserving values of δ, namely 0 and π, have been ruled out at 90% [47]. A stronger constraint on CP violation will require significantly more statistics, which is what motivates the next generation of experiments.

There has recently been a joint fit between the T2K and NOvA collaborations (Fermilab Joint Experimental/Theoretical Physics Seminar February 2024, https://indico.fnal.gov/event/62062/). The analysis points to the need for much larger statistics in order to measure both the mass ordering and the CP-violating phase. The mass ordering preferred by each experiment alone is not the same as the mass ordering preferred by the combination of the two experiments, in order to accommodate a common value of the other mixing matrix values.

4. Next steps in neutrino oscillation measurements

To get definitive measurements on the CP-violating phase and the mass ordering, the field needs experiments with significantly more statistics than what has been collected by the current generation of experiments. The difficulty in measuring the differences in oscillation probabilities also argues for using complementary approaches for these measurements.

The HyperK experiment will use a new 258 kton (total mass) Water Cerenkov detector, which has an eight times larger fiducial volume than SuperK, along with an upgraded J-PARC accelerator and beamline to 1.3 MW, providing 2.5 times higher neutrino flux than T2K. The statistical sensitivity will increase by a factor of 20 compared to T2K. A new Intermediate Water Cerenkov Detector (IWCD) will be constructed at about 1 km from the target as a near detector for HyperK to control systematic uncertainties. The HyperK detector is under construction, and the data-taking is expected to start in 2027 [13].

DUNE will use a liquid argon detector made of between two and four modules, where each module has a total argon mass of 17 kilotons. DUNE will use a new neutrino beamline at Fermilab, and the proton source is being upgraded to provide 1.2 MW, about a 30% higher proton intensity than the complex can currently deliver. Further upgrades to provide up to 2.1 MW are being planned. A near detector complex will be built 600 m from the neutrino production target. The expected statistical sensitivity of DUNE will increase by about a factor of 10 over NOvA, which is currently the largest fully active detector measuring long baseline neutrino oscillations [25, 52].

To take advantage of the increase of statistics that will come from the next generation of neutrino experiments, we will also need to have lower systematic uncertainties. This will come from better near detector strategies, and a better understanding of neutrino interactions. The next section describes these next steps, focusing on the Canadian efforts in these areas.

4.1. The HyperK project

The HyperK detector, shown in Fig. 8 (top), will be located 8 km south of the SuperK location and has the same 2.5 degree off-axis angle as SuperK from the J-PARC neutrino beam. It will be under a mountain with 650 m of rock overburden,

Fig. 8. Top: a schematic view of the HyperK detector, taken from ref. [13] and Bottom: a schematic view of one of the Deep Underground Neutrino Experiment (DUNE) Far Detector modules (which extends 58.2 m into the page), showing alternating anode (A) and cathode (C) planes, taken from ref. [53].

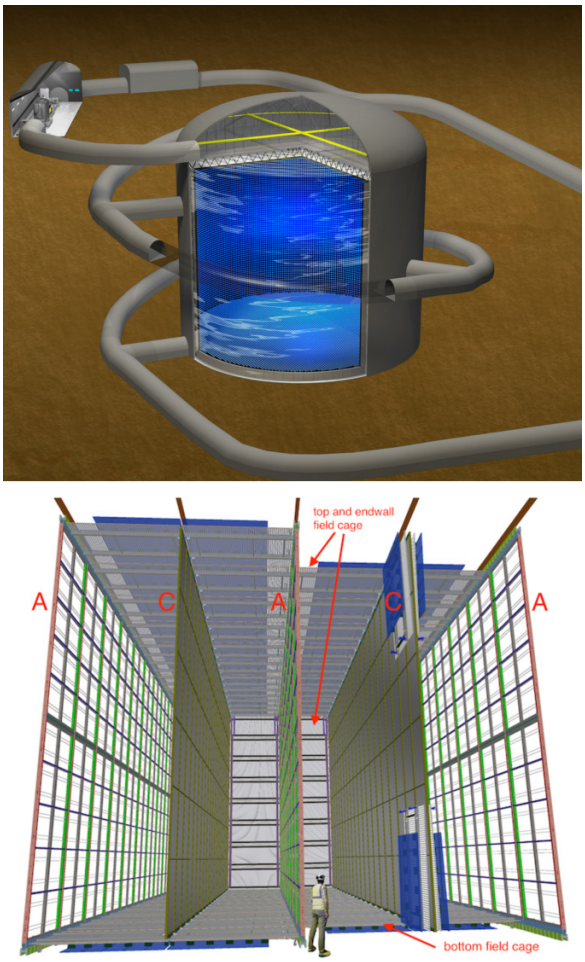

which is equivalent to 1700 m of water to shield from cosmic rays. The detector is a 258 kton Water Cerenkov detector with 187 kton fiducial volume. It has a cylindrical ultra-pure water tank of 68 m in diameter and 71 m in height. The detector structure is similar to SuperK with an eight times larger fiducial volume [13]. The HyperK detector volume is split into two sections, the inner volume that contains the signal fiducial region and an outer volume to actively shield against particles coming from outside such as the cosmic muons that survived deep underground. The inner volume surface is covered (at 20 per cent photocathode coverage) with 20 000 50 cm diameter high quantum efficiency photomultipliers (PMT). These new PMTs have a factor of 2 higher photon detection efficiency and a factor of 2 better timing resolution compared to those in SuperK for better event reconstruction.

In addition to the neutrino interaction cross-section, the detector response is the other critical area that requires significant improvement compared to SuperK. The HyperK detector will be equipped with calibration systems similar to those developed for SuperK, namely an electron linac, laser and Xenon light injectors, and Ni-Cf γ source. To improve the position-dependent calibration of the light scattering, absorption and reflection, and the PMT angular response, the HyperK detector will also be equipped with 800 multi-PMTs (mPMT), each of which consists of nineteen 8 cm PMTs housed in a 50 cm vessel. These mPMTs will precisely monitor the calibration sources with better granularity (8cm PMTs), timing resolution (1.6 ns FWHM), and angular sensitivity. The 200 mPMTs built in Canada will be equipped with 5 LED boards per mPMT, each of which has four collimated and three diffused light sources, providing a total of 7000 LED light sources (LED mPMT). The LED pulse width is less than 1 ns in width for timing calibration. The collimated light has an opening angle of 3–4 degrees to perform position-dependent light scattering, reflection, and absorption measurements. LEDs with wavelength 295 nm will be deployed for a measurement of the Raman scattering effect in which the wavelength is shifted from the deep UV below the PMT sensitivity into the sensitive region. The diffused LED will illuminate each PMT from different angles for the measurement of the angular response.

The Water Cerenkov Test Experiment (WCTE) is a small Water Cerenkov detector using mPMTs deveoped for HyperK, and is being lead by Canadian groups. The experiment will study the basic response of Water Cerenkov detectors using sub-GeV electron, muon, pion, proton, and tagged γ beams at the CERN East Hall T9 beam line [54]. The inner detector size is 3.8 m in diameter and 3.4 m in height, and is shown in Fig. 9. Multi-index aerogel Cherenkov counters have been developed to separate muons from pions for this experiment [55], and their performance is also shown in Fig. 9.

The Water Cerenkov technology works well as a calorimeter for electrons but not for sub-GeV muons. The Cherenkov light yield decreases rapidly as the muon momentum gets close to the Cherenkov threshold ($P_\mu = 120$ MeV/c). As a result, the Cherenkov light response is nonlinear to the muon energy. The WCTE will measure the relative light yield between electrons and muons to provide muon Cherenkov light yield calibration using the sub-GeV muon and electron beams. This will be important for the Δm^2_{32} measurement for mass ordering measurement in atmospheric ν_μ disappearance and the measurement of the size of the CP phase δ_{CP} in HyperK. WCTE will also measure the muon ranges and Cherenkov opening angles, which will provide independent calibration of the muon momentum. WCTE will also study the pion interactions in water, whose data is limited.

The particle identification study of electrons, muons, and pions at a high level of separation will be tested using the WCTE data. Rare failure mechanisms in particle identification will be identified to improve the simulation. The tagged γ beam will be used to study electron to gamma separation in a Water Cerenkov detector, which appears possible using machine learning combined with higher granularity mPMTs [56]. High statistics muon and electron scattering, including quasielastic scattering will be measured to constrain the neutrino interaction models.

Fig. 9. A schematic view of the Water Cerenkov Test Experiment (WCTE) detector (top) and the beam Aerogel Cherenkov data (bottom). The vertical axis is the charge in one of the counters, which is related to the index of refraction of the $\pi - \mu$ separation aerogel ($n = 1.15$ in the middle, or $n = 1.047$ at the right) and the horizontal axis is the charge in the other counter, which uses the electron veto aerogel ($n = 1.006$). Clean tagging of π and μ is achieved [55]. Image source: Mark Hartz, used with permission

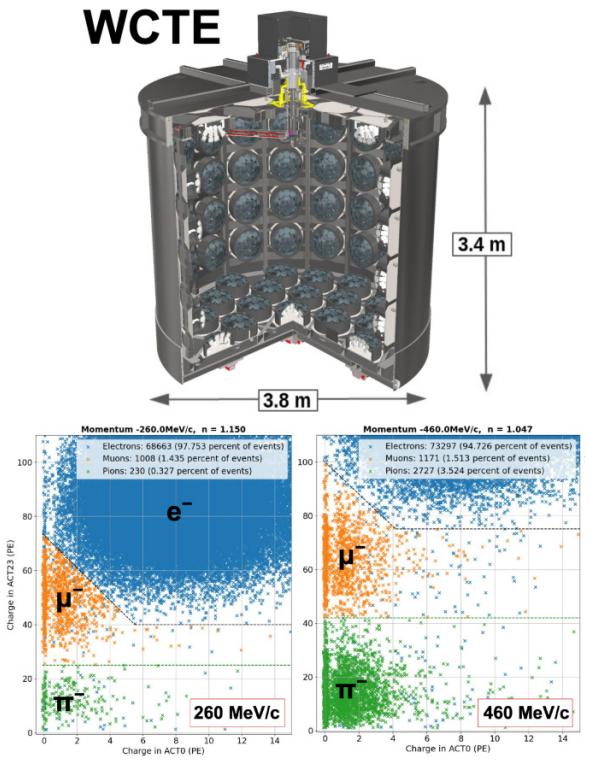

Fig. 10. Top: schematic of the horizontal drift ProtoDUNE Detector, with associated anode and cathode plane assemblies (APA, CPA, taken from ref. [58]). Bottom: energy deposition per unit length as a function of distance from the end of a track for data containing protons and muons, taken from taken from ref. [25].

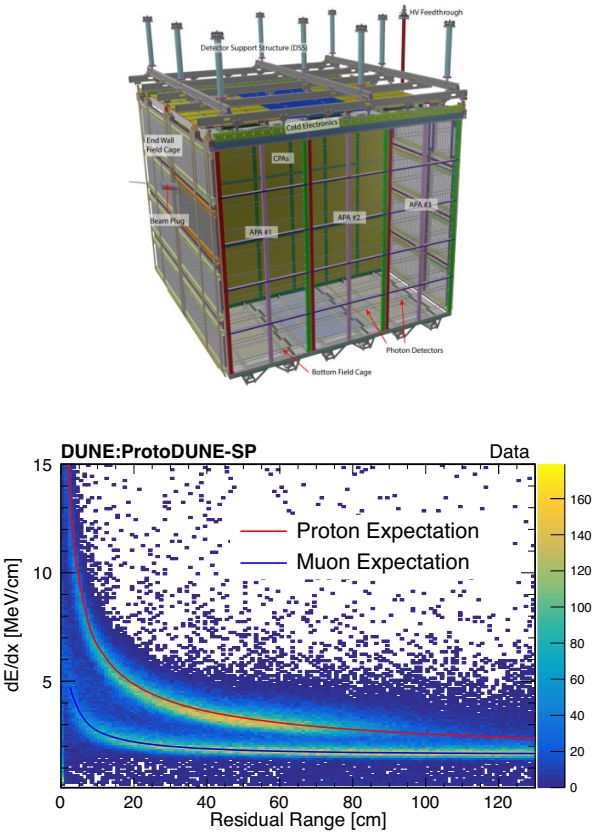

4.2. The DUNE project

The DUNE Far Detector will be made initially of two and expandable up to four cryostats measuring 15.1 m wide, 14 m high, and 62 m long. Each cryostat can contain 17 kton of liquid argon in total, resulting in at least a 10 kton fiducial volume per cryostat. There are two different configurations currently planed: one where the electric field is applied horizontally (shown in Fig. 8), and one where the field is applied vertically, so the ionized electrons are drifting either horizontally or vertically, respectively [28].

For the horizontal drift module, the drift length is 3.5 m long, and the electric field that will be provided is 500 V/cm, and is produced by applying 180 kV applied to cathode plane assemblies. The electrons will drift towards planes of wires, and the wire spacing is 5 mm to provide fine-grained information on each charged particle's trajectory [28]. For the vertical drift LAr TPC, the drift length will be 6.5 m, using an electric field of 450 V/cm supplied by a 294 kV voltage applied to the cathode plane [57]. Instead of planes of wires, the sensitive elements will be made of conducting strips printed on 3.2 mm thick printed circuit boards, where the strip will again have 5 mm spacing. The vertical drift design is easier to construct and install and reduces the cost with respect to the horizontal drift design and is being tested at the time of this writing. Subsequent module designs will be based on the upcoming test beam performance. Given the drift lengths listed above and the total drift speed of 1.6 mm/μs, the integration time for a module will need to be a few milliseconds.

The timing resolution must be good enough to have similar position resolution in the drift direction as the mm position resolution coming from the wire pitch in the directions perpendicular to the drift direction. Instrumenting such a large volume to such high granularity implies a substantial data volume. The DUNE Data Acquisition System, to which the Canadian group is heavily contributing, is essential in DUNE successfully collecting interactions in a wide-band neutrino beam as well as naturally occurring neutrino interactions.

DUNE is currently testing its far detector design by putting two large prototypes in the test beam at CERN [58], with involvement from Canadian groups. These prototypes are providing important tests of the construction strategy and also pion, proton, and kaon cross section measurements. The prototypes with the horizontal drift were already tested in a charged particle test beam at CERN, and some results are provided in ref. [25]. Figure 10 shows a schematic of the electrode structure of the horizontal drift DUNE far detector TPC proto-

type, along with a plot of the energy deposition as a function of distance from the end of both muon and proton tracks, showing clear separation between the two allowing efficient particle identification.

This provided setup gave the experiment a chance to not only measure charged particle interaction cross sections on argon, but also test the DAQ system, partially funded by a Canadian CFI JELF. The prototype has a total of 419 tons of instrumented argon, three stereo views, and a 4.67 mm wire pitch and a drift distance of 3.57 m.

5. Near detector strategies

Near detectors are key ingredients for precision oscillation measurements because of the inherent uncertainties in how many neutrinos are produced, with what energy distribution for a given neutrino beamline configuration, the uncertainties in any neutrino detector's performance, and the underlying neutrino interaction cross sections. There are therefore several requirements for a near detector: ideally a near detector would have a similar target nucleus and response to the far detector, and ideally the near detector flux would be similar in shape to the far detector flux, but would just be higher by the ratio (squared) of the two different baselines.

Both DUNE and HyperK are planning for near detectors that are a smaller version of their far detector technology that uses the same target nucleus: HyperK is planning an Intermediate Water Cerenkov Detector (IWCD) located about 1 km from the neutrino production target [13] and DUNE will build a liquid argon TPC that is located 574 m from the neutrino production target [59]. Figure 11 shows the near detector complex for DUNE (left) and the IWCD configuration for HyperK (right). In both cases, there is a near detector with an identical target material (argon or water) but because the event rates between near and far detectors are different by up to a factor of a million in both experiments, the detector sizes can be smaller. In order to get similar performance between near and far detectors, however, certain other differences are also introduced.

HyperK's IWCD detector has a 8.8 m diameter and is 11 m in height detector, and will be located in a pit that has a 10.2 m diameter and is 46.1 m deep. The inner volume is 7 m in diameter and 8 m in height, and the inner surface is covered by 370 mPMTs to make up for the smaller detector size. The smaller PMT size than the HyperK detector is required to keep the similar granularity. The J-PARC beam spill consists of eight bunches of 20–30 ns wide pulses every 1.3 s. The bunches themselves are separated by 600 ns, so all of the prompt light (not from electrons which could arise from stopped muon decays) is well separated in time in the IWCD. The IWCD event rate is expected to be at most one event per bunch at 1 km distance. By adjusting the pit water level, the IWCD detector can move to cover the off-axis angle from 1.7 degrees to 4 degrees, and efforts are underway to extend the coverage down to 1.5 degrees.

DUNE's liquid argon near detector will still be a time projection chamber, but because of the instantaneous neutrino rate at that location the active elements will be square-meter-scale planes comprised of ~4 mm × 4 mm pixels rather than

Fig. 11. Top: Deep Underground Neutrino Experiment (DUNE) Near Detector hall with the liquid and gaseous argon detectors (ND-LAr and ND-Gar, repsectively) located off the neutrino beam axis to show the range of motion [59]. The System for on-Axis Neutrino Detection (SAND) is in the downstream end of the hall. Bottom: the Intermediate Water Cerenkov Detector for HyperK [60].

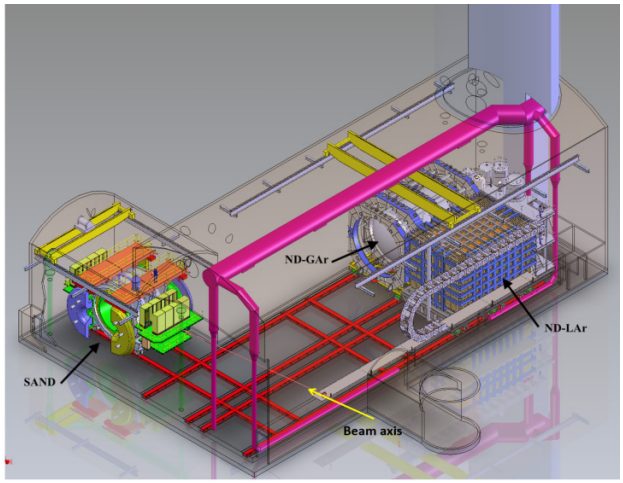

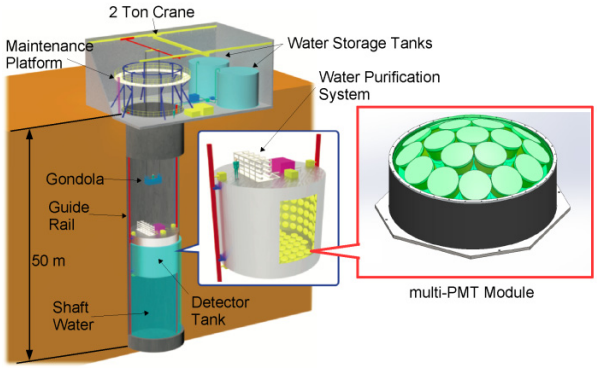

wire planes. In addition, the detector will be segmented into 35 different modules with separate light and charge readout. The detector will not be large enough to contain most muons that are produced by neutrinos at DUNE energies, so there will be a downstream muon spectrometer at the start of the DUNE run, which will later be upgraded to be a gaseous argon Time Projection Chamber. A prototype of the liquid argon near detector has been tested in cosmic ray tests as described in ref. [61] and has been commissioned underground at Fermilab in the NuMI [62] neutrino beam, where it will be tested for neutrino event reconstruction along with fast tracking detectors, similar to the near detector strategy. Figure 12 shows several examples of what cosmic rays look like in this pixellated TPC geometry. Significant Canadian effort has gone into characterizing this new detector techology with cosmic rays [61], and in testing this technology in the NuMI beam at Fermilab.

Having almost identical near and far detector technologies is not sufficient, because the $\nu_\mu \rightarrow \nu_\tau$ oscillation probability is so large at the far detector compared to the near detector, so

Fig. 12. Event displays from a cosmic ray test of the pixelated near detector technology from Deep Underground Neutrino Experiment (DUNE). Taken from ref. [61].

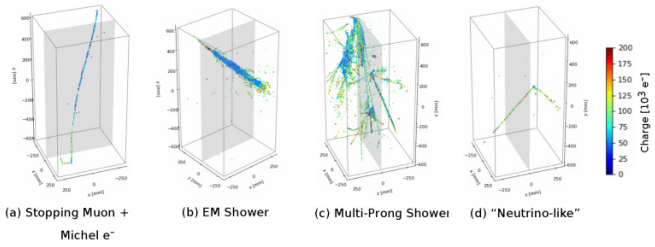

the ν_μ and $\bar{\nu}_\mu$ fluxes at the far detector will never be similar in shape to those at the near detector. In addition, because near detectors tend to be placed only a short distance away from the downstream end of the decay region, the neutrino energy spectrum even in the absence of oscillations would not be similar because of the length of the decay volume. Finally, the electron neutrino to muon neutrino flux ratio at the near detector will be smaller than that at the far detector, so understanding the ν_e to ν_μ cross section ratio at the far detector is itself challenging because the backgrounds are so different between the near and far locations.

One strategy to address the fact that the ν_μ energy spectrum is so different between the near and far detectors is the "PRISM" concept [63], which was first proposed as an addition to T2K by the Canadian group and has been adopted by both DUNE and HyperK. This concept again takes advantage of the fact that for two-body pion decays, the muon neutrino energy is uniquely determined by the pion energy and the angle between the pion direction of flight and the neutrino decay direction. By collecting neutrino event distributions as a function of visible energy with the same detector at a variety of different off-axis angles, an experiment can predict a visible energy distribution for any linear combination of the fluxes at those different off-axis angles. Both experiments are planning near detectors that can take data at a span of different off-axis angles, but will also take data with their near detectors at the same off-axis angle as the far detector (0 degrees for DUNE, and 2.5 degrees for HyperK) to estimate neutral current and intrinsic beam ν_e background rate directly. This concept is demonstrated for HyperK and DUNE in Fig. 13. The neutrino energy spectrum shifts to lower energy with a narrower width, as the off-axis angle gets larger. The off-axis angle dependence of the neutrino energy spectrum is strongly correlated by the two body pion decay kinematics to produce these neutrinos. By making a linear combination of neutrino fluxes at different off-axis positions, an almost monochromatic neutrino flux response can be studied (Fig. 13 middle). The HyperK (DUNE) near detector moves vertically (horizontally) to reach different off-axis angles.

Still another requirement for a near detector facility is to measure neutrino beam stability as a function of time. For HyperK, this will be done by a grid of scintillator/steel sandwich detectors that are centered on the beamline axis itself; the INGRID detector that has been used for T2K [64]. For DUNE this will be done by the SAND detector made of straw tubes

Fig. 13. Relationship between the off-axis position and the neutrino energy in HyperK (top) and a linear combination of neutrino flux at different off-axis positions to form a monochromatic beam (middle) [63], and Deep Underground Neutrino Experiment (DUNE)'s fluxes at different off-axis angles (bottom) [28].

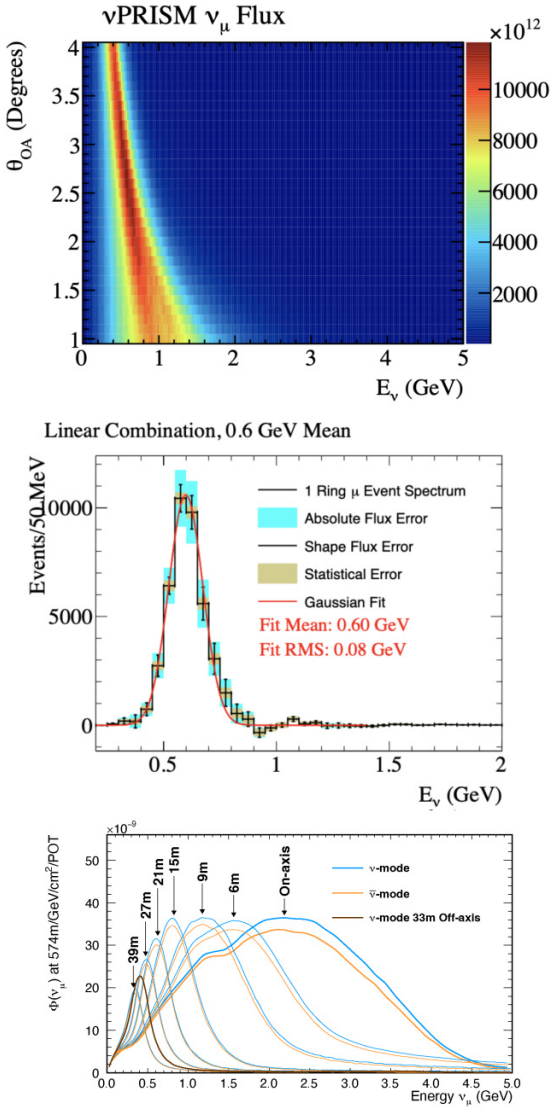

in a magnetic field, which will be located at the downstream end of the DUNE near detector hall and will remain on axis for the entire run [59].

Additional near detectors will be needed to measure neutrino interactions at even lower thresholds than the far detector. HyperK will make use of the current ND280 detector constructed by T2K, which includes a fine-grained scintillator detector that can track individual protons and pions produced well below Cherenkov threshold, placed in a magnetic field to be able to measure both the neutrino and antineutrino components in each beam configuration [65]. DUNE is planning, in a later phase of the experiment, to build a gaseous argon TPC that can look at the final state particles from neutrino interactions on argon at even lower thresholds than the liquid argon version of the detector.

Fig. 14. Expected event spectra as a function of reconstructed neutrino energy for different values of the CP-violating phase δ. From left to right, the spectra are ν_e appearance in neutrino and antineutrino mode, followed by the ν_μ disappearance in neutrino and antineutrino modes. Taken from ref. [51].

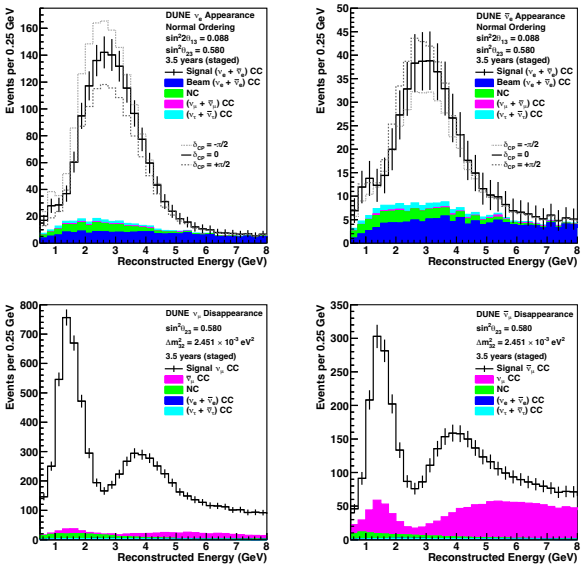

6. Expected sensitivities for oscillation measurements

Because the statistics in this next generation of experiments will eventually be factors of 10–20 larger than those of the current generation, the systematic uncertainties will have to be reduced below the several percent uncertainties that the current generation has achieved. The expected statistics are described in this section, as well as the key systematic uncertainties that must be reduced below current levels. In particular, we will focus on those uncertainties that affect the measurements of CP violation and the mass ordering, which will be done through comparisons of the $\nu_\mu \rightarrow \nu_e$ measurement and the $\bar{\nu}_\mu \rightarrow \bar{\nu}_e$ measurement.

Figure 14 shows the expected spectra in the DUNE experiment after 3.5 years of running in both neutrino and antineutrino modes, assuming a ramp up of the proton power from 1.2 to 1.8 MW and an increase in detector mass from two modules to four modules [51]. The expected event statistics for electron neutrino appearance range from 500 to 1000 events (300–500 events) for the neutrino mode (antineutrino mode) depending on the mass ordering, and represent an early opportunity to measure the mass ordering, and an opportunity to measure both the CP-violating phase and to search for non-standard neutrino interactions that could arise from neutrinos passing through 1300 km of earth.

Figure 15 shows the expected event statistics for the HyperK experiment after 2.5 years of running in neutrino and 7.5 years in antineutrino mode with a proton beam power of 1.3 MW at JPARC [13]. About 1000–2000 events each are expected for electron neutrino appearance in neutrino mode and antineutrino mode.

Fig. 15. Expected event spectra as a function of reconstructed neutrino energy for different values of the CP-violating phase δ at HyperK. From left to right, the spectra are ν_e appearance in neutrino and antineutrino mode, followed by the ν_μ disappearance in neutrino and and antineutrino modes. These statistics assume 2.5 years of running in neutrino and 7.5 years in antineutrino mode with a proton beam power of 1.3 MW at JPARC [13]. Taken from ref. [13].

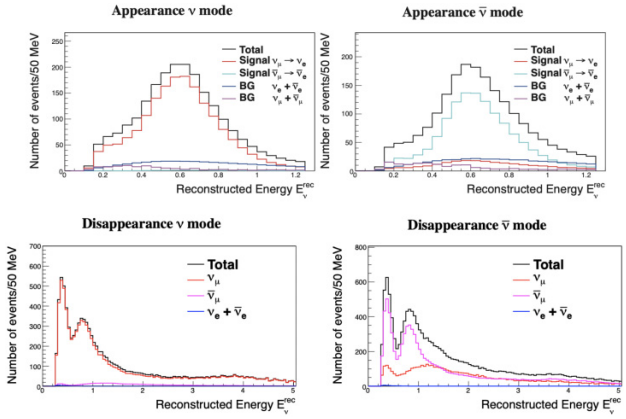

While the statistics quoted differ for the two experiments, the reach in different parameter measurements is also very different because of the different baselines and energy spectra and will ultimately depend on how low the systematic uncertainties can be. Furthermore, whether the mass ordering is inverted or normal will also affect each experiment's precision on the CP-violating phase. Conversely, for any value of δ, the DUNE experiment should be able to determine the mass ordering after a few years of running at currently achievable proton intensity rates [52].

To understand what uncertainties are important given the spectra shown above, it is useful to recall the formulae that describes the number of identified ν_μ events in the near detector (N_n)and the identified ν_e events in the far detector (N_f).

$$N_n(\nu_\mu) = \Phi_n(\nu_\mu)\,\sigma(\nu_\mu)\,M_n\varepsilon_n(\nu_\mu) + B_{n,\mu} \tag{5}$$

$$N_f(\nu_e) = P(\nu_\mu \rightarrow \nu_e)\,\Phi_f(\nu_\mu)\,\sigma(\nu_e)\,M_f\varepsilon_f(\nu_e) + B_{f,e} \tag{6}$$

where $\Phi_x(\nu_\mu)$ represents the muon neutrino flux in the absence of oscillations at either the near or far detector, $\sigma(\nu_\alpha)$ represents the neutrino CC cross section for flavour α, $\epsilon_x(\nu_\alpha)$ represents the efficiency at either the near or far detector for seeing neutrinos of flavour α. The backgrounds to electron neutrino appearance in the far detector ($B_{f,e}$) are dominated by the electron neutrinos that were produced in the beamline originally (most of which are still electron neutrinos since their disappearance probability is small), or from neutral current interactions. The backgrounds in the near detector ($B_{n,\mu}$ are small or are dominated by the wrong-sign contamination, and will be predicted using the magnetized near detectors. Detector and beamline strategies have been chosen to ensure that the backgrounds at the oscillation maximum are at the one percent level and can be well constrained using

the near detector measurements. Therefore, the systematic uncertainty on the background estimate is not expected to dominate the measurement. Furthermore, the backgrounds to muon neutrino events in the near detector are expected to be much smaller than the backgrounds to electron neutrino events in the far detector since the beam is primarily muon neutrinos (or antineutrinos). There is a similar equation for the antineutrino oscillation probability measured while the beam is in the antineutrino configuration, with corresponding fluxes, cross sections, and backgrounds ($\overline{\Phi}(\nu_x)$, $\sigma(\bar{\nu}_x)$, $\bar{B}_f$, respectively).

When one takes the ratio of the two equations above and solves for the oscillation probability, one gets the following result:

$$P(\nu_\mu \to \nu_e) = \frac{N_f(\nu_e) - B_{f,e}}{N_n(\nu_\mu) - B_{n,\mu}} \times \frac{\sigma(\nu_\mu)}{\sigma(\nu_e)} \times \frac{\Phi_n(\nu_\mu)}{\Phi_f(\nu_\mu)} \times \frac{\varepsilon_n(\nu_\mu)}{\varepsilon_f(\nu_e)} \times \frac{M_n}{M_f} \quad (7)$$

In reality, the events at both detectors will be measured as a function of the estimated neutrino energy, and the cross sections, and detector efficiencies must be convoluted over the incoming flux distribution as a function of true neutrino energy. However, if one considers for a moment what would be measured in a monochromatic neutrino beam, it is clear that certain ratios become important.

Ultimately, we are interested in the difference in ν_e appearance probability between antineutrinos and neutrinos. Since the near to far flux ratio is governed primarily by the differences in distances and the pion decay kinematics convoluted with the magnetic field of the horns, that ratio is expected to be very similar between neutrino mode and antineutrino mode. The detector mass ratios between near and far detectors should also be well known for both beamline configurations.

If we define the ratio of those two appearance probabilities as R (again at one energy), and the far to near flux ratio and the detector mass ratio are also the same, then this gives the following double ratio:

$$R \equiv \frac{P(\bar{\nu}_\mu \to \bar{\nu}_e)}{P(\nu_\mu \to \nu_e)} = \frac{N_{far}(\bar{\nu}_e) - \bar{B}_{far,e}}{N_{near}(\bar{\nu}_\mu) - \bar{B}_{near,\mu}} \times \frac{N_{near}(\nu_\mu) - B_{near,\mu}}{N_{far}(\nu_e) - B_{far,e}} \times \frac{\sigma(\nu_e)}{\sigma(\nu_\mu)} \frac{\sigma(\bar{\nu}_\mu)}{\sigma(\bar{\nu}_e)} \frac{\varepsilon_n(\bar{\nu}_\mu)}{\varepsilon_n(\nu_\mu)} \frac{\varepsilon_f(\nu_e)}{\varepsilon_f(\bar{\nu}_e)} \quad (8)$$

By simultaneously using information from both the near and far detectors, from both neutrino and antineutrino mode data, the experiments are effectively measuring the ratio of oscillation probabilities, which is directly related to the CP-violating phase δ and the mass hierarchy (in other words, whether Δm_{23} is positive or negative). Using eq. (2), and plugging in the current knowledge of the angles θ_{13}, θ_{12}, θ_{23}, the asymmetry neutrino and antineutrino oscillation probabilities at the first vacuum oscillation maximum (where E_ν[GeV] $= \Delta m^2$[eV^2]L[km]/4 $= 1.27$ can be expressed as follows [66]:

$$A = \frac{P(\nu_\mu \to \nu_e) - P(\bar{\nu}_\mu \to \bar{\nu}_e)}{P(\nu_\mu \to \nu_e) + P(\bar{\nu}_\mu \to \bar{\nu}_e)} = \frac{1-R}{1+R}$$
$$A \approx \frac{\cos\theta_{23} \sin 2\theta_{12} \sin\delta}{\sin\theta_{23} \sin\theta_{13}} \left(\frac{\Delta m^2_{21} L}{4E_\nu}\right) + \text{matter effects}$$
$$\approx -0.28 \sin\delta + \text{matter effects} \quad (9)$$

where the asymmetry due to matter effects in the absence of CP violation overall is about 0.08 for HyperK and about 0.4 at DUNE's oscillation maximum [66]. The coefficient of $\sin\delta$ in the equation is dependent on whether or not θ_{23} is above or below 45°. By using the best fit values for all the parameters given by ref. [1] and changing from $\theta_{23} = 49°$ to $\theta_{23} = 45°$, the coefficient of $\sin\delta$ in eq. (8) changes from 0.26 to 0.30. Clearly seeing CP violation is only one goal, a precise measurement of δ will require precision on all the other mixing angles.

Equation (8) provides a sense of the scale below which the systematic uncertainties must fall. The smaller the uncertainty in R, the smaller a value of δ will be measurable by each experiment. This equation also shows why it will be straightforward for DUNE to measure the mass ordering, since that effect at the oscillation maximum is already known to be larger than the effect of CP violation.

Although the neutrino and antineutrino cross sections are quite different due to parity violation in weak interactions, the electron and muon neutrino cross sections are similar thanks to the $\mu - e$ universality of the weak interaction, as are the electron and muon antineutrino cross sections. The $\mu - e$ universality in ν_e and ν_μ cross sections is broken because the lighter electron mass allows for a larger phase space in the final state and incurs larger radiative corrections. The effects are estimated to be about 10% in HyperK are expected to be a smaller effect at DUNE energies [67]. When such effects are coupled with nuclear and hadronic uncertainties, the cross section ratio becomes challenging to predict, and experimental verification becomes essential. The measurement of the cross section ratios between ν_e and ν_μ and between between $\bar{\nu}_e$ and $\bar{\nu}_\mu$ in the near detector (and elsewhere) are therefore important.

The response to muons in the near detector and the response to electrons in the far detector are also quite different from one another, but the responses for μ^+ and μ^- in the near detector as well as e^+ and e^- response in the far detector are in principle similar between the neutrino and antineutrino modes. However, the kinematics of the neutrino and antineutrino interactions are quite different due to parity violation. Charged leptons from antineutrino interactions are more strongly peaked in the antineutrino direction compared to charged leptons from neutrino interactions. Similarly, leptons from antineutrinos tend to carry a larger fraction of the antineutrino energy than do leptons from neutrino interactions. Uncertainties in the lepton angular and energy acceptance of the detector response therefore introduce an additional systematic uncertainty in the double ratio. Calibration of the energy response and uniformity in the detector position will be important in either experiment. For the liquid argon detector using the calorimetric energy reconstruction, the fraction of energy going into neutrons will be more important to estimate, since final state neutron kinetic energy is not directly measurable, but again will be correlated between muon and electron neutrinos, and correlated between muon and electron antineutrinos.

Another cross section-related difference between far and near detector event rates comes from the energy dependence

of the cross section. The neutrino cross section uncertainty directly affects the neutrino energy reconstructions in the far and near detector differently due to the difference in their energy distributions. Both experiments will study the systematic uncertainty in neutrino energy reconstruction using the "PRISM" approach by moving one of the near detectors to different off-axis positions.

Overall these challenges to precision long baseline oscillation measurements provide motivation for a rich set of neutrino interaction measurements both at future and currently operating neutrino detectors. These challenges also provide opportunities for collaboration with nuclear theorists and experimentalists and will result in a better understanding of the weak structure of nuclei.

7. Astroparticle physics using large neutrino detectors

In addition to the long baseline neutrino program, the large underground neutrino detectors are effective for a wide range of physics and astroparticle physics programs, as demonstrated by SuperK. For example, solar neutrinos can be used for the extraction of the solar neutrino oscillations, such as the transition from the matter resonance to vacuum oscillation (up-turn), and day–night asymmetry, which shows the earth matter effect in the solar neutrino oscillations. Other astrophysical neutrino measurements are described below.

One exciting possibility is the detection of a supernova burst from the Milky Way galaxy all the way to the Andromeda galaxy. The detected neutrino flux and types as a function of time would provide insight into the supernova explosion mechanism deep inside the star. The HyperK and DUNE detectors are especially complementary in this regard, because of the low energies of these neutrinos. The HyperK detector is sensitive to electron antineutrinos through inverse beta decay on the hydrogen in the water ($\bar{\nu}_e + p \rightarrow e^+ + n$), while DUNE is sensitive to electron neutrinos through the process $\nu_e + {}^{40}\mathrm{Ar} \rightarrow e^- + {}^{40}K^+$ [13, 68]. The only process available to both detectors and all neutrino flavours is neutrino-electron scattering where the final state particle is an electron coming from the source direction with less energy than the initial supernova neutrino.

DUNE and HyperK detectors are also sensitive to the neutrinos and antineutrinos, respectively, from past supernova explosions, the so-called "relic" supernova neutrinos. Their energy spectra would provide an insight into the fraction of the failed supernova explosions, which ended up into black holes instead of neutron stars after the core collapsed and stopped explosion prematurely.

Multi-GeV neutrino point sources could come from AGN and other astronomical events as well as from dark matter annihilations at the centre of the galaxy or the centre of the sun. A technical challenge for the DUNE detector that the Canadian effort is tackling is the ability to buffer all of the data produced within DUNE for 10–100 seconds before identifying a potential Supernova event and deciding to retain the data. This challenge is addressed with a flexible DAQ system, consisting of high performance servers hosting solid state drives for online retention of potential Supernova candidates [28].

8. Additional searches for beyond the standard model physics

The existence of neutrino masses and measurement of neutrino properties fits into the 3-flavour oscillation paradigm that is already beyond the Standard Model (BSM) of particle physics. In addition to these measurements, HyperK and DUNE detectors will be capable of a much broader BSM program that includes searches such as for sterile neutrinos, nonstandard interactions (NSI), PMNS nonunitarity, CPT violation, proton decay, light dark matter, boosted dark matter, neutrino-trident production, heavy neutral leptons, large-extra dimensions, and new heavily ionizing particles such as monopoles and Q-balls [13, 68]. Although the backgrounds will be very different, both experiments are sensitive to ν_τ appearance from atmospheric neutrinos, and DUNE is in addition sensitive to ν_τ appearance from the beam.

The two different experiments are also complementary in the search proton decay; HyperK is most sensitive to $p \rightarrow e\pi^0 \sim (\pi^0 \rightarrow \gamma\gamma)$ decays because of its larger mass, while the liquid argon detector has a higher efficiency for observing charged kaons from the proton decay, $p \rightarrow K^+\bar{\nu}$ [13, 68].

8.1. Nonstandard interactions

Atmospheric neutrinos, because of their very long baseline, can provide sensitive searches for non-standard Interactions (NSI), especially when combined with the beam-based measurements of HyperK and DUNE [69]. The zenith angle of the lepton is a proxy for the zenith angle of the neutrino, which direction provides the length that the neutrino traveled through the earth. A measurement of the neutrino flux as a function of inferred energy and zenith angle provides the neutrino oscillation in a large baseline length, up to 10 000 km, and neutrino energy up to 10–100 GeV. This type of measurement is called a neutrino oscillogram. The flux coming from the bottom of the detector with oscillation can be normalized to that coming from the top (without oscillation) to cancel many of the systematic uncertainties. The oscillogram is sensitive to the matter resonance effect to determine the mass ordering and detect the $\nu_\mu \rightarrow \nu_\tau$ oscillation. The wide range of neutrinoenergies and baselines accessible by atmospheric neutrinos also means broad sensitivity to NSI. The large HyperK detector expands the energy range of the fully contained atmospheric neutrino events beyond SuperK with higher statistics. While the DUNE far detectors have a lower total mass than the HyperK detector, their ability to reconstruct more about each event could potentially allow for better separation between tau neutrinos and other neutrinos, and may also be able to reconstruct neutrino-dominated samples and antineutrino-dominated samples using hadronic information.

8.2. Tau neutrinos

Only 19 tau neutrino candidates have been detected worldwide, making the tau neutrino the least measured Standard

Model particle [70–72]. Tau neutrino detection is one of the cornerstones confirming the 3-flavour paradigm and improving the discovery potential for sterile neutrinos, NSI, and PMNS nonunitary. Preliminary studies show that it will be possible to select approximately 25 tau neutrino charged current candidates per year using the DUNE beam when it is optimized to search for CP violation [73], and approximately 70 atmospheric candidates in 350 kt-year [68]. A high-energy beam optimized for tau neutrino events would provide approximately 150 charged current candidates [68], which could significantly improve constraints on nonunitarity parameters [73]. Although tau neutrinos produced in the beam occur at energies above the first oscillation maximum due to the kinematic threshold for producing a tau on shell, machine learning algorithms are being developed in order to optimize the events accessible in the high-energy region of the beam and provide DUNE with the highest statistics tau neutrino samples available [59].

9. Complemenarity between HyperK and DUNE

HyperK and DUNE are optimized for different aspects of neutrino oscillation measurements and are complementary. As outlined in this document, the two experiments have chosen very different neutrino energies (0.6 GeV compared to 2–3 GeV), different beamline strategies (off-axis narrow band beam compared to on-axis broad band beam), and different detector strategies, which imply different techniques for background rejection and neutrino energy reconstruction. Both experiments expect to collect enough statistics to measure the CP-violating phase δ over a large range of possible values, and DUNE can independently measure the neutrino mass ordering a few years after the start of operations, for all values of δ. Both experiments rely on improvements to neutrino interaction measurements to accurately predict backgrounds, and the relationship between incoming neutrino energy and what is visible in their detectors. Both experiments will rely on improvements in flux predictions coming from improved measurements of hadron production coming from experiments like EMPHATIC [74] and NA61/Shine [75].

The physics of neutrino mass and mixing is the most striking BSM physics signature in particle physics, and it is critical that we investigate this phenomenon in as many complementary aspects as possible. The efforts described here take advantage of Canadian-based expertise and the combination of the two experiments is greater than the sum of the parts.

Acknowledgements

We gratefully acknowledge the support of the Canadian Foundation for Innovation, the Natural Sciences and Engineering Research Council of Canada, TRIUMF and the National Research Council Canada under Industry Canada, and the Institute of Particle Physics. This document was prepared in part using the resources of the Fermi National Accelerator Laboratory (Fermilab), a U.S. Department of Energy, Office of Science, Office of High Energy Physics HEP User Facility. Fermilab is managed by Fermi Forward Discovery Group, LLC, acting under contract No. 89243024CSC000002. Thanks to the *Canadian Journal of Physics* for proposing this special issue.

Article information

History dates

Received: 14 June 2024
Accepted: 22 July 2024
Accepted manuscript online: 16 April 2025
Version of record online: 26 May 2025

Notes

This paper is part of a special issue entitled Astroparticle Physics in Canada.

Copyright

Data availability

This manuscript does not report data.

Author information

Author ORCIDs

Deborah A. Harris https://orcid.org/0000-0001-9469-0820

Author contributions

Writing – original draft: DH, NI, AK
Writing – review & editing: DH, NI, AK

Competing interests

The authors declare there are no competing interests.

References

1. R.L. Workman, et al. (Particle Data Group). PTEP, **2022**, 083C01 (2022). doi:10.1093/ptep/ptac097.
2. Y. Fukuda, et al. (Super-Kamiokande). Phys. Rev. Lett. **81**, 1562 (1998). doi:10.1103/PhysRevLett.81.1562.
3. Q.R. Ahmad, et al. (SNO) Phys. Rev. Lett. **89**, 011301 (2002). doi:10.1103/PhysRevLett.89.011301.
4. F.P. An, et al. (Daya Bay). Phys. Rev. Lett. **130**, 161802 (2023), arXiv:2211.14988. doi:10.1103/PhysRevLett.130.161802.
5. G. Bak, et al. (RENO). Phys. Rev. Lett. **121**, 201801 (2018). doi:10.1103/PhysRevLett.121.201801.
6. H. de Kerret, et al. (Double Chooz). Nat. Phys. **16**, 558 (2020). doi:10.1038/s41567-020-0831-y.
7. M.A. Acero, et al. (NOvA). Phys. Rev. D, **106**, 032004 (2022). doi:10.1103/PhysRevD.106.032004.
8. K. Abe, et al. (T2K). Phys. Rev. D, **108**, 072011 (2023). doi:10.1103/PhysRevD.108.072011.
9. L. Wolfenstein. Phys. Rev. D, **17**, 2369 (1978). doi:10.1103/PhysRevD.17.2369.
10. C. Jarlskog. Phys. Rev. Lett. **55**, 1039 (1985). doi:10.1103/PhysRevLett.55.1039.

11. K. Abe, et al. (T2K). Phys. Rev. Lett. **107**, 041801 (2011). doi:10.1103/PhysRevLett.107.041801.
12. F.P. An, et al. (Daya Bay). Phys. Rev. Lett. **108**, 171803 (2012). doi:10.1103/PhysRevLett.108.171803.
13. K. Abe, et al. (Hyper-Kamiokande). (2018), arXiv:1805.04163 [physics.insdet]. doi:10.48550/arXiv.1805.04163.
14. M. Giesch, B. Kuiper, B. Langeseth, S. van der Meer, D. Neet, G. Plass, G. Pluym, and B. De Raad. Nucl. Instrum. Meth. **20**, 58 (1963). doi:10.1016/0029-554X(63)90391-4.
15. D. Beavis, et al.(E899). (BNL Report Number 52459. (1995). doi:10.2172/52878.
16. I. Esteban, M.C. Gonzalez-Garcia, M. Maltoni, T. Schwetz, and A. Zhou. JHEP, **9**, 178 (2020). doi:10.1007/JHEP09(2020)178.
17. L. Pickering, R. Wendell, Y. Qiyu, and K. Skwarczynski. Available from https://github.com/rogerwendell/prob3plusplus. (2018).
18. M.V. Diwan, V. Galymov, X. Qian, and A. Rubbia. Ann. Rev. Nucl. Part. Sci. **66**, 47 (2016). doi:10.1146/annurev-nucl-102014-021939.
19. K.S. Hirata, et al. (Kamiokande-II). Phys. Lett. B, **280**, 146 (1992). doi:10.1016/0370-2693(92)90788-6.
20. Y. Fukuda, et al. (Kamiokande). Phys. Rev. Lett. **77**, 1683 (1996). doi:10.1103/PhysRevLett.77.1683.
21. K. Hirata, et al. (Kamiokande-II). Phys. Rev. Lett. **58**, 1490 (1987). doi:10.1103/PhysRevLett.58.1490.
22. C.B. Bratton, et al. (IMB). Phys. Rev. D, **37**, 3361 (1988). doi:10.1103/PhysRevD.37.3361.
23. K. Abe, et al. (T2K). Phys. Rev. Lett. **112**, 181801 (2014). doi:10.1103/PhysRevLett.112.181801.
24. R. Acciarri, et al. (MicroBooNE). JINST, **12**, P02017 (2017). doi:10.1088/1748-0221/12/02/P02017.
25. B. Abi, et al. (DUNE). JINST, **15**, P12004 (2020). doi:10.1088/1748-0221/15/12/P12004.
26. S. Amerio, et al. (ICARUS), (ICARUS). Nucl. Instrum. Meth. A, **527**, 329 (2004). doi:10.1016/j.nima.2004.02.044.
27. R. Acciarri, et al. (SBND) JINST, **15**, P06033 (2020). doi:10.1088/1748-0221/15/06/P06033.
28. B. Abi, et al. (DUNE). JINST, **15**, T08010 (2020). doi:10.1088/1748-0221/15/08/T08010.
29. W. Foreman, et al. (LArIAT). Phys. Rev. D, **101**, 012010 (2020). doi:10.1103/PhysRevD.101.012010.
30. R. Acciarri, et al. (MicroBooNE). JINST, **12**, P03011 (2017). doi:10.1088/1748-0221/12/03/P03011.
31. P. Abratenko, et al. (MicroBooNE). Phys. Rev. D, **103**, 052012 (2021). doi:10.1103/PhysRevD.103.052012.
32. S. Henry, et al. (MINERvA). (Phys. Rev. D, **109**, 092008(2024)(2023). doi:10.1103/PhysRevD.109.092008.
33. A. Olivier, et al. (MINERvA). Phys. Rev. D, **108**, 112010 (2023). doi:10.1103/PhysRevD.108.112010.
34. J. Kleykamp, et al. (MINERvA). Phys. Rev. Lett. **130**, 161801 (2023). doi:10.1103/PhysRevLett.130.161801.
35. A. Bashyal, et al. (MINERvA). Phys. Rev. D, **108**, 032018 (2023). doi:10.1103/PhysRevD.108.032018.
36. M.A. Ramírez, et al. (MINERvA). Phys. Rev. Lett. **131**, 051801 (2023). doi:10.1103/PhysRevLett.131.051801.
37. A. Bercellie, et al. (MINERvA). Phys. Rev. Lett. **131**, 011801 (2023). doi:10.1103/PhysRevLett.131.011801.
38. T. Cai, et al. (MINERvA). Nature, **614**, 48 (2023). doi:10.1038/s41586-022-05478-3.
39. A.S. Meyer, M. Betancourt, R. Gran, and R.J. Hill. Phys. Rev. D, **93**, 113015 (2016). doi:10.1103/PhysRevD.93.113015.
40. D. Ruterbories, et al. (MINERvA). Phys. Rev. Lett. **129**, 021803 (2022). doi:10.1103/PhysRevLett.129.021803.
41. K. Abe, et al. (T2K) PTEP, **2021**, 043C01 (2021). doi:10.1093/ptep/ptab014.
42. K. Abe, et al. (T2K). Phys. Rev. D, **103**, 112009 (2021). doi:10.1103/PhysRevD.103.112009.
43. K. Abe, et al. (T2K). Phys. Rev. D, **108**, 112009 (2023). doi:10.1103/PhysRevD.108.112009.
44. K. Abe, et al. (T2K). Phys. Rev. D, **108**, 092009 (2023). doi:10.1103/PhysRevD.108.092009.
45. Y. Itow, et al. (T2K). The JHF-Kamioka neutrino project. In *In* 3rd Workshop on Neutrino Oscillations and Their Origin. NOON. 2001. pp. 239–248. doi:10.48550/arXiv.hep-ex/0106019.
46. K. Abe, et al. (T2K). Nucl. Instrum. Meth. A, **659**, 106 (2011). doi:10.1016/j.nima.2011.06.067.
47. K. Abe, et al. (T2K). Eur. Phys. J. C, **83**, 782 (2023). doi:10.1140/epjc/s10052-023-11819-x.
48. H. Nunokawa, S.J. Parke, and R. Zukanovich Funchal. Phys. Rev. D, **72**, 013009 (2005). doi:10.1103/PhysRevD.72.013009.
49. S.J. Parke and R. Zukanovich-Funchal. Phys. Rev. D, **111**, 013008 2024). doi:10.48550/arXiv.2404.08733.
50. A. Abusleme, et al. (JUNO). Chin. Phys. C, **46**, 123001 (2022). doi:10.1088/1674-1137/ac8bc9.
51. B. Abi, et al. (DUNE). Eur. Phys. J. C, **80**, 978 (2020). doi:10.1140/epjc/s10052-020-08456-z.
52. A. Abud Abed, et al. (DUNE), Phys. Rev. D, **105**, 072006 (2022). doi:10.1103/PhysRevD.105.072006.
53. B. Abi, et al. (DUNE), JINST, **15**, T08008 (2020). doi:10.1088/1748-0221/15/08/T08008.
54. R. Akutsu, et al. (WCTE). CERN Report SPSC-2020-005. (2020).
55. A. Craplet. (WCTE). Poster at the 12th Beam Telescopes and Test Beams Workshop. (2024).
56. P.D.P. Nicholas Prouse and W. Fedorko. Phys. Sci. Forum, **8**, 63 (2023). doi:10.3390/psf2023008063.
57. A. Abed Abud, et al. (DUNE). JINST, **19**, T08004 (2024). doi:10.1088/1748-0221/19/08/T08004.
58. A. Abed Abud, et al. (DUNE). JINST, **17**, P01005 (2022). doi:10.1088/1748-0221/17/01/P01005.
59. V. Hewes, et al. (DUNE). Instruments, **5**, 31 (2021). doi:0.3390/instruments5040031.
60. M. Hartz. (Hyper-Kamiokande). Presentation at ICHEP 2020. (2020).
61. A. Abed Abud, et al. (DUNE). (2024). doi:10.48550/arXiv.2403.03212.
62. P. Adamson, et al. Nucl. Instrum. Meth. A, **806**, 279 (2016). doi:10.1016/j.nima.2015.08.063.
63. S. Bhadra, et al. (nuPRISM). (2014). doi:10.48550/arXiv.1412.3086.
64. K. Abe, et al. Nucl. Instrum. Meth. A, **694**, 211 (2012). doi:10.1016/j.nima.2012.03.023.
65. K. Abe, et al. (T2K). (2019). doi:10.48550/arXiv.1901.03750.
66. M. Bass, et al. Phys. Rev. D, **91**, 052015 (2015). doi:10.1103/PhysRevD.91.052015.
67. O. Tomalak, Q. Chen, R.J. Hill, K.S. McFarland, and C. Wret. Phys. Rev. D, **106**, 093006 (2022). doi:10.1103/PhysRevD.106.093006.
68. B. Abi, et al. (DUNE). (2020). doi:10.48550/arXiv.2002.03005.
69. J. Rout, M. Masud, and P. Mehta. Phys. Rev. D, **95**, (2017). doi:10.1103/PhysRevD.95.075035.
70. DONUT Collaboration. Phys. Lett. B, **504**, 218 (2001). doi:10.1016/S0370-2693(01)00307-0.
71. OPERA Collaboration. Phys. Rev. Lett. **120**(2018). doi:10.1103/PhysRevLett.120.211801.
72. Super-Kamiokande Collaboration. Phys. Rev. Lett. **110**(2013). doi:10.1103/PhysRevLett.110.181802.
73. A. de Gouvêa, K.J. Kelly, G.V. Stenico, and P. Pasquini. Phys. Rev. D, **100**(2019). doi:10.1103/PhysRevD.100.016004.
74. M. Pavin, et al. (EMPHATIC). Phys. Rev. D, **106**, 112008 (2022). doi:10.1103/PhysRevD.106.112008.
75. H. Adhikary, et al. (NA61/SHINE). Phys. Rev. D, **108**, 072013 (2023). doi:10.1103/PhysRevD.108.072013.